A polaron approach to photorefractivity in Fe : $LiNbO_3$

A polaron approach to photorefractivity in $Fe : LiNbO_3$

Laura Vittadello,[1,*] Marco Bazzan,[1] Anush Danielyan,[2] Edvard Kokanyan,[2,3] Laurent Guilbert,[4] and Michel Aillerie[4]

[1] *University of Padova, Physics and Astronomy Department, Via Marzolo 8, 35131, Padova, Italy*

[2] *Institute for Physical Research, National Academy of Sciences of Armenia, Ashtarak-2, 0203, Armenia*

[3] *Armenian State Pedagogical University after Kh. Abovyan, Tigran Metsi Ave., 17, Yerevan, Armenia*

[4] *Laboratoire Matériaux Optiques, Photonique et Systèmes, Université de Lorraine et CentraleSupélec, 2 rue E. Belin, F-57070 Metz, France*

Abstract

The thermally activated, incoherent hopping of small electron polarons generated by continuous illumination in iron-doped lithium niobate is simulated by a Marcus-Holstein model for which all the input parameters are known from literature. The results of the calculations are compared with a comprehensive set of data obtained from photorefractive, photogalvanic and photoconductive measurements under green light excitation on samples with different doping levels and stoichiometries in the temperature range between 150 K and room temperature. We show that the temperature and composition dependence of the photorefractive observables can be interpreted by a change in the abundance of the different hop types that a polaron performs before being captured by a deep Fe trap. Moreover, by a comparison between experimental and numerical data we obtain new insights on the initial photo-excitation part of the photorefractive process. In particular all results are consistent if a single value of the photogalvanic length $L_{PG} = (1.44 \pm 0.05)$ Å is assumed for all the samples and all the temperatures. The photo-generation efficiency ϕ under green light excitation (somewhere denoted as *quantum efficiency*) is also estimated. It appears to decrease from 10-15% at room temperature to about 5% at 150K. This behavior is qualitatively interpreted in terms of a temperature-dependent re-trapping probability of the light-emitted particles from the initial Fe donor center.

*Present Affiliation: School of Physics, Osnabrueck University, Barbarastrasse 7, 49076, Osnabrueck, Germany

I. INTRODUCTION

Lithium niobate ($LiNbO_3$, LN) is often taken as a paradigm for light induced charge transport phenomena in polar oxide crystals. This is the physical basis of the so-called photorefractive effect, which in LN is especially strong as a consequence of the high electro-optic coefficients and of the fact that large internal electric fields ($10^6 - 10^7 V/m$) can be built up in the bulk simply by illuminating this material with visible low intensity light [1]. Those phenomena bear a high interest for practical applications: in the field of non-linear and ultra-fast optics the photorefractive effect limits the use of LN for high intensity processes [2], while in photorefractive holography it is used to record high quality gratings, optical memories and demonstrate low-intensity all-optical interactions [3]. Integrated optics as well needs to control those phenomena due to the high cw light intensities obtained in wave-guiding regions [4]. In more recent approaches, the space charge field was exploited to manipulate nano-sized materials [5] or to operate liquid-crystal photorefractive cells [6]. Additionally, the exploding field of ferroelectric photovoltaics has attracted a strong interest in understanding charge transport processes in polar materials [7].

The microscopic origin of those internal electric fields is related to the interplay between the photogalvanic effect (i.e. the appearance of a bulk current density proportional to the photon flux) and the charge transport mechanisms that determine the material conduction [8]. Both those phenomena have been described in the past by mutuating from semiconductor physics a band model picture embodied by the well-known Kukhtarev-Vinetskii equations [9].

However, more recently, charge transport phenomena in LN:Fe has been interpreted in terms of small polarons creation and migration [10]. In the initial stage of the process, some charge carriers are photo-generated from deep donor centers and emitted with a preferential direction in the conduction band. Subsequently those "hot" carriers lose energy by interaction with the lattice and finally condensate into a new state which is self-localized by a distortion of the local ionic environment. Under certain conditions the carrier, localized at a single lattice site, and the surrounding deformation can be thought as a quasi-particle that moves as a whole: the small polaron. Its motion takes place by thermally assisted hopping transitions to adjacent sites [11]. It is therefore mandatory to update the description of light - induced charge transport phenomena incorporating the polaron physics.

In Fe:LN the initial step of the photo - transport process relies on poorly known phenomenological parameters: the *photogalvanic length* L_{PG} and the *photo-generation efficiency* ϕ (sometimes indicated also as *quantum efficiency*). The former can be interpreted as the average position from the donor center at which a newly emitted charge condensates into a polaron. The fact that this average is different from zero in absence of an applied field is the very origin of the photogalvanic effect. The second parameter ϕ indicates that not all the absorbed photons succeed in creating a polaron contributing to the photogalvanic effect.

On the other hand, the second step of the photo - transport process, i.e. the incoherent hopping transport of small polarons, can be modeled by means of the Marcus-Holstein model [12, 13]. It has been shown [14] that by using few parameters obtainable from spectroscopic measurements this model can successfully reproduce the polaron transport in a wide composition and temperature range by means of Monte Carlo simulations dealing with the different polaronic centers present in LN:Fe.

The aim of the present work is therefore to compare experimental data obtained on a set of samples with different compositions and between room temperature and 150 K with Monte Carlo simulations based on the Marcus-Holstein hopping model. From the comparison a quantitative estimation of L_{PG} and ϕ will be obtained, as well as some insights on how the observed dependencies can be interpreted in terms of polaron hopping.

II. EXPERIMENTAL

A. Macroscopic Observables

In the following we consider the simplest experimental situation of a Fe:LN sample illuminated with a uniform strip of light (see Figure 1). The c axis is supposed to be parallel to the input surface and perpendicular to the illuminated strip, to realize a quasi 1-D configuration. In these conditions a refractive index change is observed as a consequence of the buildup of a light-induced space charge field and of the electro-optic effect [3, 15]. Thus, the main quantities of interest in describing the photo - transport in Fe:LN are essentially three: (i) the photogalvanic current initiating the buildup of the field; (ii) the material's conductivity under illumination; (iii) the stationary space charge field, proportional to the maximum refractive index change. Those quantities will be briefly discussed in the next

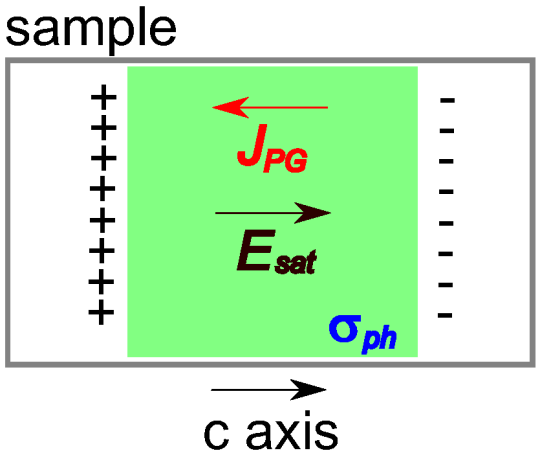

Figure 1:

(Colors online) Scheme of the experimental geometry: a Fe:LN sample is illuminated with a uniform strip of light. Inside the illuminated volume a current density j_{PG} and a conductivity σ_{PC} are established. The charge accumulation at the boundaries of the illuminated area give rise to an electric field E_{sat} that in stationary conditions counterbalances the photogalvanic current.

sessions in the context of polaron transport. We developed an all-optical setup, described in the Supporting Information, which allow for a measure of those three quantities without the need for electrical connections and as a function of temperature. The macroscopic observables were then systematically measured on a set of six samples presented in forthcoming paragraphs.

1. *Photogalvanic current*

In the case of the 1D problem described above, the photogalvanic current is directed essentially along the c axis and can be written in scalar form [1, 10] as:

$$j_{PG} = \kappa \alpha I = qsN \frac{I}{h\nu} \phi L_{PG} \tag{1}$$

where q is the charge of the photo-excited carriers, $\alpha = sN$ is the absorption coefficient (with s the cross section and N the concentration of the photogalvanic centres, respectively), I is the light intensity, $h\nu$ the photon energy and L_{PG} the photogalvanic length. ϕ is the photo-generation efficiency factor, i.e. the probability to create a charge contributing to the current

from an absorbed photon, appearing also in the expression for the photoconductivity (see next section). Since all the parameters involved in the photo-generation rate $G = qsN\frac{I}{h\nu}$ are known, it is convenient to normalize the experimentally measured j_{PG} with respect to$G$, obtaining what we may call the effective photogalvanic length:

$$L_{PG}^{eff} = \frac{j_{PG}}{G} = \phi L_{PG} \tag{2}$$

It should be noted that usual experiments provide access to this quantity, but not to ϕ and L_{PG} separately.

2. Photoconductivity

The photoconductivity σ_{ph} is generally expressed [3] as:

$$\sigma_{ph} = q\mu n = qsN\frac{I}{h\nu}\phi\mu\tau \tag{3}$$

In this equation μ is the drift mobility of the light - induced carriers, n their concentration and τ their lifetime. The last equivalence is derived from a band-like description using a rate-equation system [3]. It is important to note that this expression requires two fundamental assumptions (i) the charge carriers are normally diffusing particles characterized by a time-independent mobility; (ii) the carrier decay time is described by an equation of the kind $dn/dt = -\frac{1}{\tau}nN^+$, where N^+ is the concentration of ionized donors acting also as deep traps, $[Fe^{3+}]$ in our case. Both those assumptions are fully reasonable in a band model, but when dealing with polaron transport they need more careful verification. Normal diffusion laws may not be verified [16] for a polaron hopping on a defective lattice with a distance- and energy- dependent attempt frequency. On the other hand, a rate equation such as the one used in band models entails the mono-exponential decay of a carrier population, while it is known (see e.g. [2]) that polaron decays are rather described by stretched exponential functions (Kohlrausch - Williams- Watts law) owing to a heavy-tailed distribution of trapping times.

Those observations indicates that in the polaron context it is challenging knowing or even defining μ and τ separately. However, as already observed by Sturman et al. [17], the above mentioned problems can be overcome considering that what is needed here is not μ, nor τ in isolation but the quantity that in a band model is given by the product $\mu\tau$ i.e. the average

distance $\langle z \rangle$ run by a polaron under a unitary electric field from its creation to its trapping. Differently from μ and τ in isolation, this quantity can be operatively defined also in our context:

$$\Lambda = \langle z \rangle / E \tag{4}$$

and can be straightforwardly computed by a Monte Carlo approach. It should be noted that the $\langle z \rangle$ displacement of a hopping particle under electric field and after a given time remains proportional to the electric field magnitude under very general conditions, including anomalously diffusing particles [16] so that the definition is robust.

The photoconductivity (normalized for the photo-generation rate G) is thus given in terms of Λ:

$$\Sigma = \frac{\sigma_{ph}}{G} = \phi\Lambda \tag{5}$$

3. Space charge field

Under homogeneous cw-light exposure, charge carriers tend to move along the c axis due to the photogalvanic effect. Charge accumulation outside illuminated areas gives rise to the build-up of a space charge field in the material. Assuming that diffusion currents and dark conductivity are negligible, as it is appropriate in the experimental conditions adopted in this work, the saturation value of the electric field E_{sat} is attained when, after an initial transient, the photogalvanic current, Eq. 1, is counterbalanced by the drift current $j_{drift} = \sigma_{ph}E$. From Eqs. (1, 3) one has:

$$E_{sat} = \frac{j_{PG}}{\sigma_{ph}} = \frac{L_{PG}}{\Lambda} \tag{6}$$

The initial transient of the space charge field evolution, for our simple 1D geometry, follows a simple exponential law [3, 15]:

$$E(t) = E_{sat}\left(1 - e^{-t/\tau_d}\right) \tag{7}$$

The time constant τ_d in Eq. (7) is the so-called dielectric relaxation time, given by:

$$\tau_D = \frac{\varepsilon\varepsilon_0}{\sigma_{ph}} \tag{8}$$

and provides a direct access to the sample photoconductivity σ_{ph}.

B. Samples

Two series samples were grown for this work. The first one is composed of congruent samples (Nb/Li ratio equal to 0.94) but with different iron concentrations (Series sample A), grown by Czochralski technique at the University of Padova (Italy). This series of samples is conceived to study the effect of different trap concentrations. The Fe contents in the melt was chosen equal to 0.02 mol%, 0.05 mol% and 0.1 mol%. The second sample series (referred as B) is the one having a fixed deep trap concentration but a different amount of shallow traps (i.e. niobium antisites). In particular three samples, doped with Fe 0.11 mol%, with different stoichiometry were grown at the Institute for Physical Research in Ashtarak (Armenia). High-purity compounds of Nb_2O_5 from Johnson-Mattley, and Li_2CO_3 from Merck, in powder form, were used as the starting materials for sintering of the lithium niobate charges of different composition, via solid state reaction. The appropriate amount of iron was added to the initial charges of LN in the form of Fe_2O_3 oxide (Merck) and thoroughly mixed. This kind of growth is known to produce samples with a composition which is not constant along the growth direction. Therefore the precise composition of the final samples cannot be assumed to be equal to the one of the melt and need to be characterized. All the samples were X-ray oriented, cut and optically polished in parallelepipeds with typical sizes of some millimeters per side.

The Fe^{2+} absolute concentration is obtained from the optical absorption at $\lambda = 532\,\mathrm{nm}$ as proposed by Berben *et al.* [18]. Assuming that, for weak doping levels as the ones used here, the total Fe concentration in the crystals is the same as in the melt, the amount of Fe^{3+} traps present in the samples is obtained by difference. The concentration of Nb_{Li} antisite defect can be estimated by Raman spectroscopy [19–21] since a linear relationship between the Li deficiency and the broadening of Raman peaks was established. All the samples of the series B were measured in the X(zz)X backscattering configuration using a LabRAM Aramis Micro-Raman spectrometer, in order to obtain the $A_1(TO_1)$ modes, corresponding to Nb/O vibrations in x-cut samples [22]. The modes were fitted by Lorentzian functions in order to measure their FWHM Γ and from the equation [21]:

$$X_C = 69.39 - 0.123 \times \Gamma_{A_1(TO_1)} \tag{9}$$

the molar concentration $X_C = \frac{[Li]}{[Li]+[Nb]}$ can be obtained. However, in this work a different instrument with respect to the one mentioned in [21] was used, so the formula 9 has to be

sample name	X_C%	$[Nb_{Li}]$	$[Fe_{tot}]$	$[Fe^{2+}]$	$[Fe^{3+}]$	R%
		$10^{25}\,m^{-3}$	$10^{25}\,m^{-3}$	$10^{25}\,m^{-3}$	$10^{25}\,m^{-3}$	
A/0.34/19.0	48.45	19.0	0.37	0.04 ± 0.01	0.34 ± 0.1	10.9 ± 0.3
A/0.82/19.0	48.45	19.0	0.95	0.12 ± 0.01	0.82 ± 0.02	14.3 ± 0.3
A/1.56/19.0	48.45	19.0	1.89	0.33 ± 0.01	1.56 ± 0.07	21.1 ± 0.4
B/1.84/19.0	48.45	19.0	20.9	0.24 ± 0.01	1.84 ± 0.01	13.08 ± 0.09
B/1.78/17.5	48.58 ± 0.03	17.5	20.9	0.31 ± 0.01	1.78 ± 0.05	17.2 ± 0.5
B/1.94/6.4	49.49 ± 0.03	6.4	20.9	0.15 ± 0.01	1.94 ± 0.02	7.6 ± 0.1

Table I: Summary of compositional parameters for the two groups of samples investigated. In the last column the reduction ratio $R = [Fe^{2+}] \,/\, [Fe^{3+}]$ is also reported.

checked. The spectral line profile used in this analysis is Lorentzian which width is due to the "true" Raman line shape convoluted with a "instrumental" function, which depends on the instrument used, on the wavelength etc. As the convolution of two Lorentzian functions is again a Lorentzian whose width is equal to the sum of the widths of the two functions, it can be considered that a change in the setup may affect only the intercept of equation 9, while the slope may be considered as accurate. To estimate the correct intercept, a reference sample is needed. The congruent composition is by definition the one in which the crystal composition is equal to the melt composition and can be expected to be the one with the highest compositional uniformity. In the following therefore the samples grown from the congruent melt are considered as reference and their composition is assumed by default.

The results of those characterizations are reported in Table I. In the following, to indicate a sample we adopt the labelling convention: Series/Deep Traps (in $10^{25}\,m^{-3}$)/Shallow Traps (in $10^{25}\,m^{-3}$). Thus for example, the label A/0.34/19.0 indicates the sample of the series A with a Fe^{3+} concentration of $0.34 \times 10^{25}\,m^{-3}$ and a Nb_{Li} antisite defect content of $19.0 \times 10^{25}\,m^{-3}$.

III. THEORY AND SIMULATION

A. Microscopic model

LN hosts four different kinds of intrinsic small polarons [23]: the free polaron (FP) Nb_{Nb}^{4+}, the bound polaron (GP) Nb_{Li}^{4+}, the bipolaron (BP) Nb_{Nb}^{4+} : Nb_{Li}^{4+}, and the hole polaron (HP) $O^- - V_{Li}$. Electrons bound to Fe_{Li}^{3+} may also be described in the framework of the strong-coupling-polaron picture. Hole polarons are produced at visible wavelengths by high intensity pulsed beams by two-photon processes and will not be considered here, as in our Fe doped samples and at cw intensities the electron generation from Fe^{2+} is by far predominant. Moreover, in Fe-doped samples, bipolarons are not observed because the system tends to relax to the more stable Fe defect, so in the following we will disregard also this centre. In conclusion, we will assume that in the dark the sample does not contain free or bound polarons and that all the charges are stored in Fe^{2+} centres. When a photon in the visible range is absorbed by a Fe^{2+} donor, a small electron polaron is created. It performs a certain number of hops either on Nb_{Nb} or on Nb_{Li} sites until it is re-trapped at a deep Fe_{Li}^{3+}trap, which defines the final distance run by the particle.

B. Polaron transport in Fe:LN

According to the Marcus - Holstein polaron hopping model [11–13], the non-adiabatic hopping frequency for a $(i \to f)$ hop is:

$$w_{i,f}(r,T) = \frac{1}{2}\left(\frac{\pi}{kT\lambda_{i,f}}\right)^{\frac{1}{2}} \frac{I_{i,f}^2}{\hbar} \exp\left(-\frac{r}{a_{i,f}} - \frac{U_{i,f}}{kT}\right) \tag{10}$$

In Eq. (10), r is the distance between initial and final sites and kT the absolute temperature (in energy units). $\lambda_{i,f}$ is the reorganization energy of Marcus' theory corresponding to the energy paid to rearrange the lattice, here equal to $(E_i + E_f)$, sum of the elastic energies of the two polarons; $a_{i,f}$ is an orbital parameter describing the overlap between the electronic wave functions at site i and f. The 1/2 factor is due to the fact that Eq. (10) expresses the individual rate to a given final site, and is thus one half of the total rate in Holstein's molecular chain [13]. $U_{i,f} \neq U_{f,i}$ is the hopping barrier, given by [24, 25]:

$$U_{i,f} = \frac{(2E_i + \varepsilon_i - \varepsilon_f)^2}{4\,(E_i + E_f)} \tag{11}$$

parameter	value	unit	ref.	note
E_{FP}	0.545	eV	[23]	Free polaron energy
E_{GP}	0.75	eV	[14]	Bound polaron energy
E_{Fe}	0.7	eV	[23]	Fe defect energy
ε_{FP}	0	eV		Free polaron pre-localization energy
ε_{GP}	0.2	eV	[14]	Bound polaron pre-localization energy
$\varepsilon_{\mathrm{Fe}}$	1.22	eV	[23]	Fe defect pre-localization energy
$a_{FP,FP} = a_{GP,GP} = a_{GP,FP} = a_{FP,GP} = a$	1.6	Å	[14]	Hopping parameter
$a_{FP,\mathrm{Fe}} = a_{GP,\mathrm{Fe}} = c$	1.3	Å	[14]	Trapping parameter
$I_{FP,FP} = I_{FP,GP} = I_{GP,FP} = I_{GP,GP} = I$	0.1	eV	[27]	Transfer integral pre-factor

Table II: : Parameters used for the simulation (see text).

with ε_i and ε_f the pre-localization energies of the electron at zero deformation. When the hop occurs between sites of the same type ($i = f$), $U_{i,i} = E_i/2$, recovering the standard result that the hopping activation energy is one half of the polaron energy [2, 23, 26]. The pre-exponential factor $I_{i,f}$ describes the intrinsic hopping rate between the two sites and is determined by the choice of the (i, f) combination. According to this model, each of the three centers here considered (two Nb- based polarons, $\mathrm{Nb_{Li}}$ and $\mathrm{Nb_{Nb}}$ and the $\mathrm{Fe^{2+/3+}}$ defect) and the hopping combinations between them are described by a set of parameters. According to some recent results [14], the parameters choice reported in Table II provides a fair description of all the possible hopping processes in Fe:LN, and will be used throughout this work.

The effect of the space-charge field $\mathbf{E}$ on the hopping frequency is described by adding in Eq. (11) the term $q(\mathbf{r}_i - \mathbf{r}_f) \cdot \mathbf{E}$ inside the parenthesis at the numerator, with $\mathbf{r}_{i(j)}$ the position vectors of the starting (final) site. It is important that the field is not too strong to maintain the character of random diffusion in our simulation. In other words, the potential energy $q(\mathbf{r}_i - \mathbf{r}_f) \cdot \mathbf{E}$ gained by the polaron must remain small with respect to kT. Our field is therefore set at $5 \times 10^6\,\mathrm{V/m}$ for all the temperatures, a compromise between the above

-mentioned requirement and the necessity to observe a measurable displacement. The field is directed along the crystallographic c direction to mimic our experimental geometry.

It should be recalled that the hopping formula (10) is valid only in the non-adiabatic approximation [11] which holds whenever the transfer integral $J_{i,f}(r) = I_{i,f}^2 \exp(-r/2a_{i,f})$ is much smaller than the reorganization energy $\lambda_{i,f} = (E_i + E_f)$. By using the values reported in Tab. II we can check that this condition is well satisfied for all the hop types considered in our model. Moreover the approximation requires the lattice to possesses sufficient thermal energy to follow the charge motion and, as a rule of thumbs, is considered safe for temperatures above $\Theta_D/2$ where $\Theta_D \approx 503\,\mathrm{K}$ is the Debye temperature for lithium niobate [28]. However, experimental results obtained by Faust et al. [29] show that the the Arrhenius behaviour of the mobility in antisite-free LN is preserved till 150 K, indicating that the non-adiabatic approximation in LN holds at least down to this temperature.

C. Monte Carlo simulation

The simplest numerical approach consists in simulating one single electron at time. This situation corresponds to a low electron density system where interaction between electrons can be ignored. The electron, randomly placed at an initial $\mathrm{Nb_{Nb}}$ site, performs a walk in a structure reproducing the LN lattice. The code generates a random defect configuration in a $80 \times 80 \times 80$ super-cell of the LN structure with periodic boundary conditions, in which the polaron is launched and the position at which it is captured by a Fe^{3+} trap is recorded. The different defect concentrations of the various samples are set in accordance with Tab. I. The code computes the rest time on each visited site and the next destination site according to Eqs. (10, 11) by a classical Gillespie algorithm, as explained in ref. [25]. The probability to hop from a site i to a site f is computed as:

$$p_{i,f} = \frac{w_{i,f}}{\sum_f w_{i,f}} \tag{12}$$

where the summation at the denominator goes on all the possible destination sites inside a suitably defined volume surrounding the starting site. The simulation is repeated for a sufficient number of times, in order to compute the average distance $\langle z \rangle$ along the field direction run by the particles before being captured. From Eq. (4) the value of Λ is calculated for the different samples and for all the experimental temperatures.

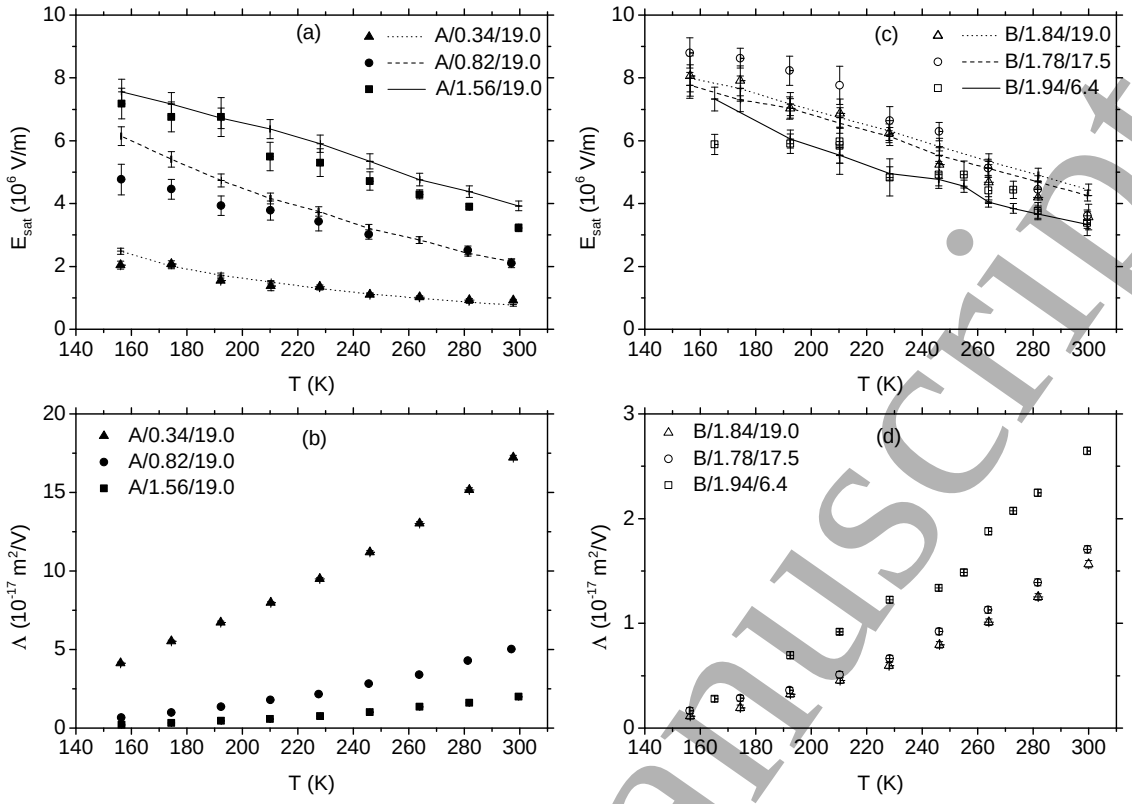

Figure 2: (a) Saturation space charge field as a function of temperature for sample series A. Dots: experimental points; Lines: recomputed results taking $L_{PG} = 1.44\,\text{Å}$ and $\Lambda_0 = 1.69 \times 10^{-17}\,\text{m}^2/\text{V}$ (see text for details). (b) Simulated Λ for sample series A. (c) Same as (a) for sample series B. (d) recomputed Λ for sample series B.

IV. RESULTS

A. Space charge field and photogalvanic length

In Figure 2 (a), (c) are reported the experimental results (dots) for the saturation space charge field value E_{sat} as a function of temperature for sample series A and B. The field shows a monotonous increase by decreasing the temperature.

The central result of our simulation is the drift coefficient Λ, i.e. the mean distance covered by a polaron under a unitary electric field from its birth to its trapping. In Figure 2 (b), (d) the simulation results obtained in the same conditions as in (a), (c) are shown. The Λ value becomes smaller and smaller by decreasing the temperature, indicating that

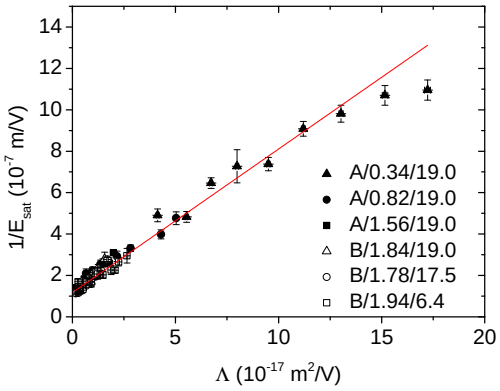

Figure 3: (Colors online) Correlation plot of experimental $1/E_{sat}$ values against simulated Λ for all the measurements. The red line is a linear fit of the data.

at low T the polaron is able to cover on average a smaller distance. By increasing the trap concentration in sample series A, Λ is decreased as well, as it can be expected (Figure 2 (b)). The effect of the antisite concentration in sample series B (2 (c)) is somehow less evident, due to the high Fe concentration that in the temperature range here explored keeps always Λ below $3 \times 10^{-17}\,\mathrm{m^2/V}$ (note the different ranges in the ordinates of (b) and (c)). However a trend is visible indicating that a higher antisite concentration hinders the charge motion or, conversely, by increasing the Li content towards stoichiometry Λ is increased.

In Figure 3 is shown the correlation plot between the reciprocal of the measured saturation space charge field $1/E_{sat}$ and the Λ values simulated for the corresponding experimental conditions. A linear correlation is recovered for almost all the samples, as it can be expected by the reciprocal of Eq. (6), $E_{sat}^{-1} = \Lambda/L_{PG}$, and by the observation that L_{PG} is an intrinsic parameter of the Fe:LN system which should be almost independent from temperature and composition [10]. Thus, the fact that almost all our data converge on a unique line can be considered as a self-consistency test. However a nonzero Λ_0/L_{PG} intercept is clearly evident from the graph. This can be interpreted as a parasitic contribution to the sample conductivity. Since this contribution appears to add up to to all the samples and for all the temperatures, this feature is likely to be an extrinsic contribution e.g. some unwanted leakage perhaps facilitated by the contact with the metallic sample holder inside our cryostat system. We note here, however, that few points relatives to the sample A/0.34/19.0 at high temperatures appear to deviate from the linear behaviour. Our data do not allow at the

moment deciding whether this is an artifact or the indication that in a range of experimental conditions wider than the one here considered the description becomes more complicated. As the large majority of our data is in agreement with the simple description of Eq. (6), we will stick here to this model, with the caveat that further work is needed to confirm their validity out of the conditions here explored.

From the linear fit of Figure 3 we retrieve $L_{PG} = (1.44 \pm 0.05)$ Å and $\Lambda_0 = (1.69 \pm 0.07) \times 10^{-17}\,\mathrm{m^2/V}$. From those values and from the results of the simulations, the saturation space charge field was re-computed by Eq. (6) for all the experimental conditions here examined and reported in Figure 2 (a) and (c) as solid lines. To our knowledge, this is the first direct comparison between temperature- and composition- dependent data in photorefractive Fe:LN and the calculations obtained from a microscopic polaron model in which no free parameters besides L_{PG} and Λ_0 were used.

B. Photoconductivity and photo-generation efficiency

In Figure 4 (a) and (c) are reported the experimental values of the specific photoconductivity Σ (dots). Combining them with the determination of L_{PG} and from the measured values of E_{sat} it is possible to estimate the photo-generation efficiency ϕ as a function of temperature. In fact, from Eqs. (2, 5, 6) one gets easily $\phi = j_{PG}/GL_{PG} = E_{sat}\Sigma/L_{PG}$. The results are reported in Figure 4 (b) and (d). All the data are coherent among the different samples: ϕ appears to decrease by cooling the sample from a value of 10 - 15% at room temperature to about 5% at low T.

By comparison, we recompute Σ according to Eq. 5 using the obtained values of ϕ, the simulated values for Λ and the correction for the leakage Λ_0, i.e. $\Sigma = \phi\,(\Lambda + \Lambda_0)$. The results are plotted in Figure 4 (a) and (c) as solid lines, showing that again all the description is consistent.

V. DISCUSSION

A. Drift Coefficient

The interpretation in terms of polaron hopping of the temperature and composition dependence of the photorefractive phenomena opens up a rich scenario, in which the interplay

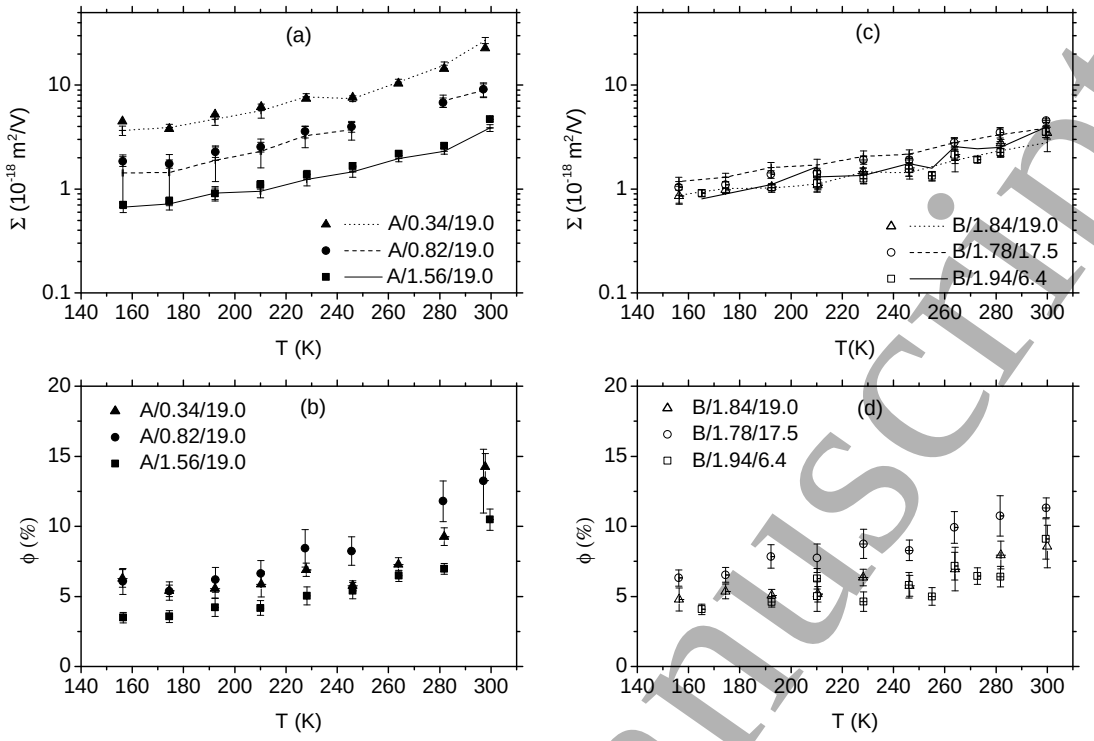

Figure 4: (a) Experimental results (dots) for the specific photoconductivity Σ for sample series A. By comparison the values obtained from our simulation corrected for the empirical values of ϕ and Λ_0 are shown (broken lines). (b) Photogeneration efficiency ϕ for the sample series A. (c) Experimental results (dots) for the specific photoconductivity Σ for sample serie B. By comparison the values obtained from our simulation corrected for the empirical values of ϕ and Λ_0 are shown (broken lines). (d) Photogeneration efficiency for sample serie B.

between the different defect centers determines the drift coefficient Λ and ultimately the main photorefractive observables.

Our simulation provides access to Λ. The decrease of this parameter with temperature (see Figure (2) (b), (d)) is due to the fact that, as a general rule, by decreasing the temperature the polarons perform a smaller number of hops to get trapped by a Fe ion [25]. It should be noted that in a hypothetical material with no Nb_{Li} antisites and vanishing Fe concentration this would not be the case. In this situation the only charge carriers would be free polarons performing a given number of hops before being trapped by a deep trap. The conduction would be ensured by thermally activated hopping among equal sites character-

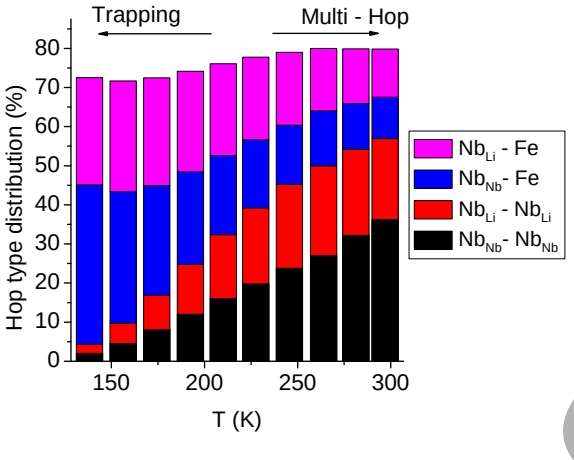

Figure 5: (Colors online) Distribution of the different hop types as a function of temperature in congruent sample A/0.82/19.0 calculated using the parameters of Tab II. Only transport ($Nb_{Nb} \rightarrow Nb_{Nb}$ and $Nb_{Li} \rightarrow Nb_{Li}$) and trapping ($Nb_{Nb} \rightarrow Fe$ and $Nb_{Nb} \rightarrow Fe$) processes are reported, the others being inefficient "conversions" $Nb_{Li} \rightleftharpoons Nb_{Nb}$ in which the polaron jumps back and forth between the same sites.

ized by a single activation energy. Therefore the temperature term of the Marcus-Holstein frequency, Eq. (10), would be the same for all hopping processes and could be simplified out from Eq. (12). This proves that the random walk performed by the polaron in this case is not affected by temperature, which would only speed up or slow down the hopping frequency, but would not change the number of hops and the distance run under the field before being trapped. The situation is different for a material with defects. In this case the starting and destination sites may be of different kind so that the hopping barriers may not be the same for all the hopping processes. The thermal part of the hopping frequency therefore cannot be simplified in Eq. (12) which becomes temperature dependent. Therefore, in material containing defects a change in temperature, besides modifying the speed of the hopping process, influences also the random walk of the particle. In particular, at sufficiently low temperatures and for the Fe concentrations used in this work, the hopping frequency of the trapping processes $Nb_{Nb}(Nb_{Li}) \rightarrow Fe$ becomes dominant with respect to the others, leading to an increase of the trapping probability upon decreasing T.

For a given sample composition we may therefore distinguish two limiting hopping regimes, upon cooling down from room temperature (or above): (i) Multi-hop, mixed trans-

port regime: the thermal budget is so high that all the hopping processes occur more or less frequently and the polaron performs several hops before being captured by a Fe^{3+} trap. In this regime the drift coefficient Λ depends strongly on the relative amount of the different hop types; in particular, at high temperatures and/or low antisite concentrations the free polaron jumps $Nb_{Nb} \rightarrow Nb_{Nb}$ dominate the transport [14]. (ii) Trapping regime: at sufficiently low temperatures, the hopping frequency towards Fe traps becomes higher than for all other processes, so that direct trapping becomes the most likely event. The two situations are illustrated in Figure 5 where the average percentage of the different hop types over the total hop number has been computed from our simulation code for sample A/0.82/19.0 as an example.

The simulations show that in these conditions the trapping can occur even if the trap is quite far away from the newborn polaron, i.e. several tens of Angstroms. A useful way to visualize this process is the concept of *trapping radius* firstly introduced in Ref. [25]. The trapping probability can be estimated by comparing the hopping frequency towards the Fe donor against the frequency towards any other center. As the hopping frequency (Eq. (10)) depends both on distance and on temperature, one can ask what is the distance $d(T)$ from a neighboring Fe center under which the polaron is more likely to be trapped than to hop away, for a given T. By some simple considerations detailed in ref. [25], it turns out that this distance obeys an equation of this kind:

$$d(T) = A + B\frac{U}{kT} \tag{13}$$

and increases from about 20 to 40 Å by decreasing T from room temperature to 150 K. The onset of the trapping regime can thus be visualized by imagining that each trap is surrounded by a finite "capture volume" with a trapping radius that increases by cooling down the sample. At low T the trapping volumes start to fill most of the available space, so that the polarons are captured within few hops.

B. Photogalvanic length

Schirmer et al. [10] gave a comprehensive revision of the photogalvanic effect in Fe:LN reinterpreting it within the polaron model. The initial direction along which the charge is emitted as a Bloch wave is determined by the Fermi golden rule, the different matrix elements

of the transition being determined by the geometrical arrangement of the ions surrounding the donor centre. In this vision the photogalvanic length L_{PG} in Eq. (1) corresponds to the averaging along the c-axis of the distance covered in the different directions prior to the polaron formation. The electron is supposed to move several $\mathrm{Nb_{Nb}} - \mathrm{Nb_{Nb}}$ distances coherently along the c axis before the lattice relaxes around it to form a $\mathrm{Nb_{Nb}^{4+}}$ small polaron state.

Our data show a consistency with the Marcus-Holstein model if a value of $L_{PG} = (1.44 \pm 0.05)$ Å is assumed. In accordance with microscopic considerations, this parameter appears to be independent on the sample and on the temperature for the range of experimental conditions explored in this work. The quantitative result is in reasonable agreement with previous tentative estimates [10] which gave L_{PG} in the Angstrom range for Fe excitation with visible light. This value may be compared with the diffusion distance that a newly emitted "hot" electron travels before condensate into a polaron, which is much larger and estimated around 23 Å [10] on average. This means that the photo-excited charge is emitted nearly isotropically and that the nonzero average displacement is only a tiny fraction of the distance run by the electron wave before the self-localization.

C. Photogeneration Efficiency

The results obtained on different samples are consistent between them and point out that ϕ is between 10 and 15% at room temperature and decrease to 5% at 150 K. In ref. [30] it is reported that ϕ decreases of about 4 times by increasing the wavelength λ from the blue to the green. Since ϕ cannot be larger than 1, in our experiments with $\lambda = 543$ nm we must have $\phi < 0.25$, in accordance with our data.

According to the model for emission of photo-excited charges mentioned in the precedent paragraph, after the initial thermalization stage the polaron is formed at a certain distance from its donor site according to some probability distribution with a mean equal to L_{PG} and a width of the order of 20 Å. The particle has now two possible choices to continue its life: to move away or to jump back to the same initial site it came from, both processes being thermally activated but with a different energy barrier. This provides a microscopic interpretation for the parameter ϕ introduced in Eq. (1), which denotes here the probability for the polaron to *not* go back to the starting site [31]. As explained above, at low

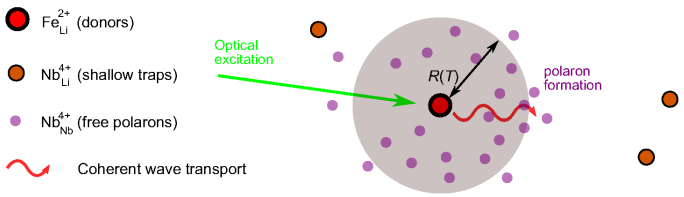

Figure 6: (Colors online) Proposed scheme for the interpretation of the photogeneration efficiency. The grey circle represents the volume where the newly formed polarons are likely to be retrapped by the Fe donor. The polarons can form at any distance from the donor center with a given probability distribution (see text).

temperature the trapping become more efficient and this can be visualized by considering that the trapping radius $R(T)$ of the Fe centers increases at low T. The trapping radius is of the order of 20 Å at room temperature, i.e. of the same order of magnitude of the diffusion distance of the hot polaron. The low value of the photo-generation efficiency is therefore explained by the fact that a large part of the polarons are formed inside the trapping radius and are thus recaptured by the same Fe donor they came from (see Figure 6).

The effect of the temperature can be easily understood as the trapping radius increases by lowering T, as a consequence of the temperature dependence of the hopping frequencies, so that the chance to escape is smaller and smaller. The increase of the photo-generation efficiency with the wavelength reported in [30] can be easily interpreted in this framework as well, considering that more energetic photons are able to project the photo-emitted charge at a longer distance from the Fe center [10]. It would be interesting to push this analysis to a more quantitative modeling, but for this aim it would be necessary to know the probability distribution function for the formation site of the polarons around the donor center. Further work is in progress to investigate this idea.

VI. CONCLUSIONS

The charge transport processes inherent to photorefractivity in Fe:LN are of two kinds: the first is the coherent motion as a conduction band state of a newly emitted charge upon absorption of a photon. The second is the localization of the charge at a single lattice site and its incoherent hopping among regular and/or defective sites. In this work we modeled

the second part of the process by means of a Marcus-Holstein hopping model, in which all the parameters were fixed by *a priori* known parameters. This allow us to calculate explicitly the incoherent transport without any assumption.

In parallel, by means of a dedicated experimental setup and tailored samples, we collected a comprehensive set of data on the photogalvanic, photoconductive and photorefractive properties as a function of the sample composition and in the temperature range between 150 K and room temperature to test the model previsions.

We showed that the experimental data and the numerical simulations are consistent with each other if a value of (1.44 ± 0.05) Å independent on the temperature and on the composition is assumed for the photogalvanic length, i.e. the average distance from the donor center at which the photo-emitted charges localize into a polaron. Moreover, by comparison with photoconductivity data, we can obtain an estimate for the photo-generation probability ϕ for Fe^{2+}under green light excitation, which amounts to about 10 % at room temperature, decreasing to 5% at 150 K. Both those quantities appear to be independent on the sample composition within our experimental accuracy and for the conditions here reported. This is, to our knowledge, the first direct quantitative estimation of those parameters related to the photo-generation process. The obtained values are in line with previous heuristic estimations reported in literature. It should be noted that the Marcus-Holstein analysis here validated for the wavelength of 543 nm could be extended to obtain information for other wavelengths, helping to investigate the dependence of the L_{PG} and ϕ upon the photon energy. Further work is needed to verify those findings for higher transport lengths.

Besides those quantitative results, our analysis provides an interpretation of the observed dependencies in the framework of the polaron model. In particular it was found that, as a general rule, by cooling the sample (for a given trap density) the number of hops and the distance run by the particle under an electric field decrease. This phenomenon, not explained by standard formulation of photorefractive equations, is a direct consequence of the combined temperature/distance dependence of the Marcus-Holstein frequency, which favors at low temperature hopping transitions towards distant Fe traps. It turns out that at sufficiently low T, the largest part of the photo-excited carriers are all trapped within few hops, entering what we may denote as "trapping" regime as opposed to the "multi-hop" regime at high temperatures. The same phenomenon accounts for the observed decrease of the photogeneration probability ϕ with T. In this respect, ϕ is thus interpreted as the

complementary of the probability that the photo-induced charge is recaptured by the same Fe donor which it came from.

Lastly, we stress how the Marcus-Holstein model was proven to possess the capability to predict the photorefractive properties of Fe:LN starting from microscopic parameters that were obtained from optical absorption and pump-probe transient absorption spectroscopy [14, 23]. In principle the same predictive capability could be used to preview the photorefractive behavior of any dopant in a given concentration and even in presence of a co-dopant, once that the microscopic parameters of the new impurities are tuned by means of few targeted experiments. This would provide a powerful tool for crystal growers helping to design new crystal compositions with tailored properties, without undergoing the time-consuming process of synthesis and testing of a large number of samples.

Acknowledgments

This research was funded by the University of Padova, grant number BIRD174398. L.V. and M.B. acknowledge Dr. N. Argiolas and L. Bacci at the University of Padova for invaluable technical assistance as well as the CloudVeneto infrastructure for providing the necessary resources for numerical simulations.

[1] A. M. Glass, D. von der Linde, and T. J. Negran. High voltage bulk photovoltaic effect and the photorefractive process in $LiNbO_3$. *Applied Physics Letters*, 25(4):233–235, 1974.

[2] M. Imlau, H. Badorreck, and Ch. Merschjann. Optical nonlinearities of small polarons in lithium niobate. *Applied Physics Reviews*, 2(4):040606, 2015.

[3] P. Günter and J.-P. Huignard. *Photorefractive Materials and Their Applications 1*, volume 113 of *0342-4111*. Springer New York, 2006.

[4] M. Bazzan and C. Sada. Optical waveguides in lithium niobate: Recent developments and applications. *Applied Physics Reviews*, 2(4):040603, 2015.

[5] M. Carrascosa, A. García-Cabañes, M. Jubera, J.B. Ramiro, and F. Agulló-López. $LiNbO_3$: A photovoltaic substrate for massive parallel manipulation and patterning of nano-objects. *Applied Physics Reviews*, 2(4):040605, 2015.

[6] L Lucchetti, K Kushnir, A Zaltron, and F Simoni. Light controlled phase shifter for optofluidics. *Optics letters*, 41(2):333–335, 2016.

[7] Ji. He, C. Franchini, and J. M. Rondinelli. Lithium niobate-type oxides as visible light photovoltaic materials. *Chemistry of Materials*, 28(1):25–29, 2016.

[8] B. I. Sturman and V.M. Fridkin. *The Photovoltaic and Photorefractive Effects in Noncentrosymmetric Materials*. Clarendon, Oxford, 1996.

[9] N. V. Kukhtarev, V. B. Markov, S. G. Odulov, M. S. Soskin, and V. L. Vinetskii. Holographic storage in electrooptic crystals. I. steady state. *Ferroelectrics*, 22(1):949–960, 1978.

[10] O. F. Schirmer, M. Imlau, and C. Merschjann. Bulk photovoltaic effect of $LiNbO_3$: Fe and its small-polaron-based microscopic interpretation. *Phys. Rev. B*, 83:165106, Apr 2011.

[11] D. Emin. *Polarons*. Cambridge University Press, 2013.

[12] R. A. Marcus. On the theory of oxidation-reduction reactions involving electron transfer. I. *The Journal of Chemical Physics*, 24(5):966–978, 1956.

[13] T. Holstein. Studies of polaron motion. *Annals of Physics*, 8(3):343 – 389, 1959.

[14] L. Guilbert, L. Vittadello, M. Bazzan, I. Mhaouech, S. Messerschmidt, and M. Imlau. The elusive role of Nb_{Li} bound polaron energy in hopping charge transport in Fe : $LiNbO_3$. *Journal of Physics: Condensed Matter*, 30(12):125701, 2018.

[15] J. Frejlich. *Photorefractive Materials: Fundamental Concepts, Holographic Recording and Materials Characterization*. Wiley, 2006.

[16] R. Metzler and J. Klafter. The random walk's guide to anomalous diffusion: a fractional dynamics approach. *Physics Reports*, 339(1):1–77, 2000.

[17] B. Sturman, M. Carrascosa, and F. Agullo-Lopez. Light-induced charge transport in $LiNbO_3$ crystals. *Physical Review B*, 78(24):245114, 2008.

[18] D. Berben, K. Buse, S. Wevering, P. Herth, M. Imlau, and Th. Woike. Lifetime of small polarons in iron doped lithium niobate. *Journal of Applied Physics*, 87(3):1034–1041, 2000.

[19] K. Lengyel, Á. Péter, L. Kovács, G. Corradi, L. Pàfalvi, J. Hebling, M. Unferdorben, G. Dravecz, I. Hajdara, Zs. Szaller, and K. Polgár. Growth, defect structure, and THz application of stoichiometric lithium niobate. *Applied Physics Reviews*, 2(4):040601, 2015.

[20] Y. Okamoto, Ping-chu Wang, and J. F. Scott. Analysis of quasielastic light scattering in $LiNbO_3$ near T_C. *Phys. Rev. B*, 32:6787–6792, Nov 1985.

[21] Y. Zhang, L. Guilbert, P. Bourson, K. Polgár, and M. D. Fontana. Characterization of short-

range heterogeneities in sub-congruent lithium niobate by micro-Raman spectroscopy. *Journal of Physics: Condensed Matter*, 18(3):957, 2006.

[22] V. Caciuc, A. V. Postnikov, and G. Borstel. Ab initio structure and zone-center phonons in $LiNbO_3$. *Phys. Rev. B*, 61:8806–8813, Apr 2000.

[23] O. F. Schirmer, M. Imlau, C. Merschjann, and B. Schoke. Electron small polarons and bipolarons in $LiNbO_3$. *Journal of Physics: Condensed Matter*, 21(12):123201, 2009.

[24] A. Zylbersztejn. Thermally activated trapping in fe-doped $LiNbO_3$. *Applied Physics Letters*, 29(12):778–780, 1976.

[25] I. Mhaouech and L. Guilbert. Temperature dependence of small polaron population decays in iron-doped lithium niobate by monte carlo simulations. *Solid State Sciences*, 60:28 – 36, 2016.

[26] I. G. Austin and N. F. Mott. Polarons in crystalline and non-crystalline materials. *Advances in Physics*, 50(7):757–812, 2001.

[27] A. Dhar and A. Mansingh. Optical properties of reduced lithium niobate single crystals. *Journal of Applied Physics*, 68(11):5804–5809, 1990.

[28] S. C. Abrahams, J. M. Reddy, and J. L. Bernstein. Ferroelectric lithium niobate. 3. single crystal X-ray diffraction study at 24Â°C. *Journal of Physics and Chemistry of Solids*, 27(6):997 – 1012, 1966.

[29] B. Faust, H. Müller, and O. F. Schirmer. Free small polarons in $Fe : LiNbO_3$. *Ferroelectrics*, 153(1):297–302, 1994.

[30] R. Grousson, M. Henry, S. Mallick, and S. L. Xu. Measurement of bulk photovoltaic and photorefractive characteristics of iron doped $LiNbO_3$. *Journal of Applied Physics*, 54(6):3012–3016, 1983.

[31] J. Carnicero, M. Carrascosa, G. García, and F. Agulló-López. Site correlation effects in the dynamics of iron impurities Fe^{2+}/Fe^{3+} and antisite defects $Nb_{Li}^{4+}/Nb_{Li}^{5+}$ after a short-pulse excitation in $LiNbO_3$. *Phys. Rev. B*, 72:245108, Dec 2005.